Weak Water Vapor Spectral Lines in the 8-12 μm Atmospheric Window

D. C. Tobin, H. E. Revercomb, R. O. Knuteson, and W. F. Feltz
Cooperative Institute for Meteorological Satellite Studies
Space Science and Engineering Center
University of Wisconsin
Madison, Wisconsin

F. J. Murcray
University of Denver
Denver, Colorado

Introduction

Weak water vapor spectral lines within the 8-μm to 12-μm atmospheric window are used for several high spectral resolution remote sensing applications, including the determination of surface temperature and emissivity, and the determination of cloud top height, temperature and emissivity of low clouds. If known accurately, these spectral lines can also be used to improve the absolute accuracy of remotely sensed water vapor by constraining the integrated total column water vapor. The Atmospheric Radiation Measurement (ARM) suite of instruments at the Southern Great Plains (SGP) (Stokes and Schwartz 1994) site in Oklahoma, armed with accurate high-resolution radiance observations and accurate knowledge of the atmospheric state, provides a unique setting for assessing and refining the spectral parameters (strength, position, and Lorentz width and shift) of these lines.

In this paper, clear-sky case studies from the 1997 Water Vapor Intensive Observation Period (WVIOP) (Revercomb et al. 1998) at the ARM SGP site are constructed using ground-based downwelling radiance spectra from the University of Wisconsin Atmospheric Emitted Radiance Interferometer (AERI) (Revercomb et al. 1994) and the higher spectral resolution version of the University of Denver (AERI-X) (Murcray et al. 1996) instruments and atmospheric state information from radiosondes, tower-based in situ observations with chilled mirrors at 25 meters and 60 meters, Microwave Radiometer (Liljegren et al. 1997), and Raman Lidar (Ferrare et al. 1995). Line-by-line calculations are performed using various spectral line data sets and the residuals are used to determine the absolute accuracy of the spectral lines and the relative accuracy from one line to the next. The calculations are also iterated to retrieve strength/width parameters for each line and these are compared to the documented values.

Applications

The “on-line/off-line” technique for retrieval of surface temperature and emissivity relies upon the accurate knowledge of the 8-μm to 12-μm water lines. Considering the clear-sky, up-welling radiative transfer equation and solving for the surface emissivity:

$$\varepsilon = \frac{B^{\uparrow}_{obs} - B^{\uparrow}_{atm} - F\downarrow \cdot \tau}{\left(B(T_s) - F\downarrow \cdot \tau\right)}$$

where $B^{\uparrow}_{obs}$ is the total up-welling radiance, $B^{\uparrow}_{atm}$ is the up-welling radiance due to atmospheric emission, $F^{\downarrow}$ is the down-welling flux at the surface, $B(T_s)$ is the radiance of the surface at temperature T_s, and τ is the surface to space (or observation altitude) transmission. For regions of low atmospheric emission and absorption, this expression simplifies to $\frac{B^{\uparrow}_{obs}}{B(T_s)}$. In practice, $B^{\uparrow}_{obs}$ is measured from aircraft or satellite and the other terms are computed using a measured or retrieved atmospheric state. The simultaneous ε, T_s retrieval is then performed by determining the T_s for which ε has no (or minimal) spectral line structure, assuming that the frequency dependence of ε is much slower than the spectral lines. This technique, which is applicable to cases in which the surface is the ground or a cloud, is illustrated in Figure 1. Figure 2 presents sample retrievals from the aircraft-based High resolution Interferometer Sounder (HIS) (Smith et al. 1990) and the polar orbiting Interferometric Monitor of Greenhouse gases (IMG) (Shimota et al. 1999) over sea ice north of Pt. Barrow, Alaska, at different times of the year. The accuracy and robustness of the on-line/off-line approach relies on the accuracy of the computed terms in the equation above, and thus on the accuracy of the line parameters of the weak lines present in this spectral region. Incorporating this type of retrieval and properly accounting for the variability, both spectrally and spatially, of the surface temperature and emissivity is important for atmospheric sounding of the boundary layer over land.

Two other applications that require explicit dependence upon the accuracy of these line parameters include the constraint of integrated column water vapor within atmospheric retrievals performed from high resolution ground-based measurements such as AERI and AERI-X, and the remote sensing of boundary layer temperature and water vapor from aircraft and satellite. A dramatic example of the later application is shown in Figure 3, where IMG observations and line-by-line calculations show the presence of a strong, low altitude inversion.

Measurements

Spectral Radiance Measurements

Ground-based, high spectral resolution radiance measurements are well suited for the evaluation and determination of the water vapor line parameters since the majority of the atmospheric emission is from ambient atmospheric pressure and temperature and thus the near-line behavior of the detected radiance is purely Lorentzian. Measurements used in this analysis are from the zenith viewing AERI (3 μm to 20 μm at 0.48^{-1} resolution) and AERI-X (7 μm to 16 μm at 0.06 cm^{-1} resolution) instruments at the SGP Cloud and Radiation Testbed (CART) site collected during the 1997 WVIOP. The absolute calibration of both instruments is 1% of ambient radiance.

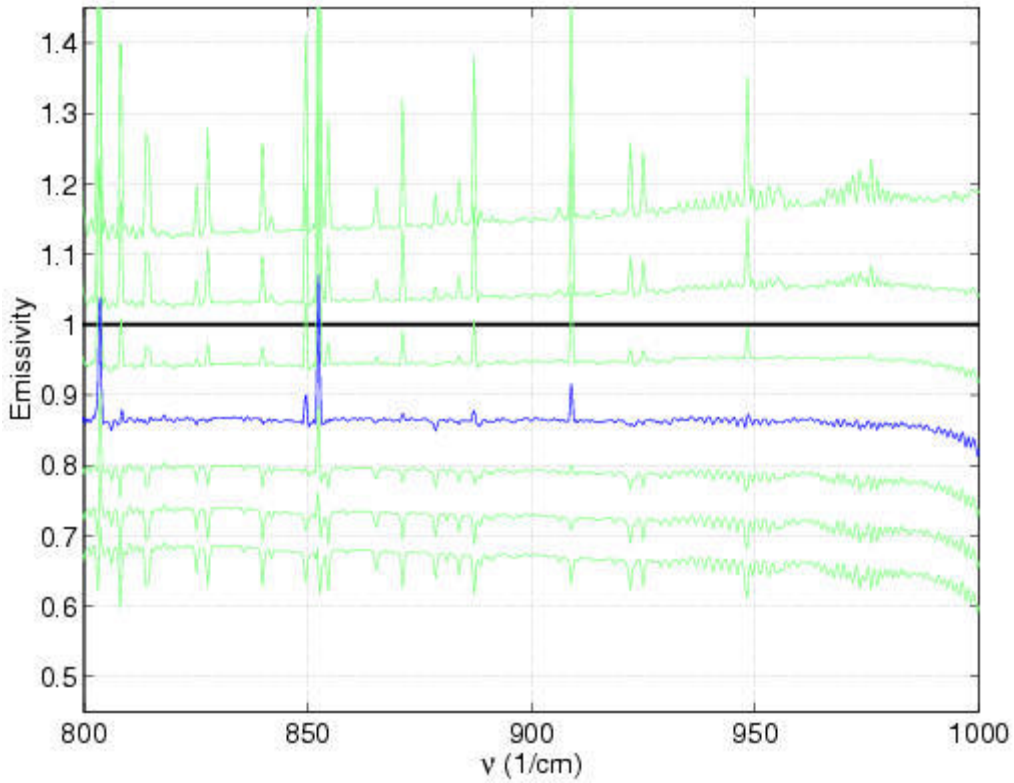

Figure 1. Illustration of the on-line/off-line surface temperature/emissivity retrieval method from aircraft. This example is from the First ISCCP (International Satellite Cloud Climatology Program) Regional Experiment-Aerosol Characterization Experiment (FIRE-ACE) campaign on May 20, 1998, using radiance observations from the HIS at 20 km over sea ice near the Surface Heat Budget of the Arctic (SHEBA) (Moritz et al. 1993) ice station and atmospheric state information from a radiosonde. The seven curves from top to bottom are the derived emissivity for assumed surface temperatures of 260 K to 290 K in 5 K increments.

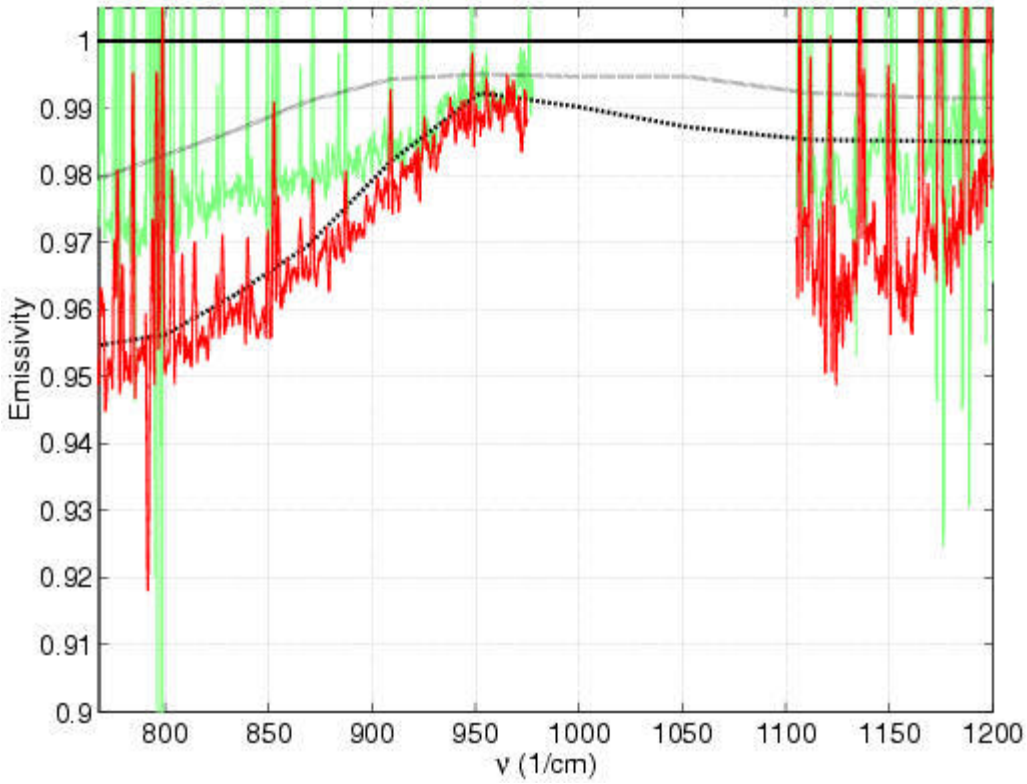

Figure 2. Sea ice emissivities derived from HIS at 20 km near the SHEBA ice station on May 20, 1998, (solid gray curve) and from IMG aboard the polar orbiting Advanced Earth Observing System (ADEOS) satellite over sea ice north of Pt. Barrow, Alaska, on December 11, 1996, (solid black curve) using the on-line/off-line retrieval technique, and laboratory measurements (Salisbury et al. 1994) of coarse granular crust (dashed curve) and wet granular snow (dotted curve).

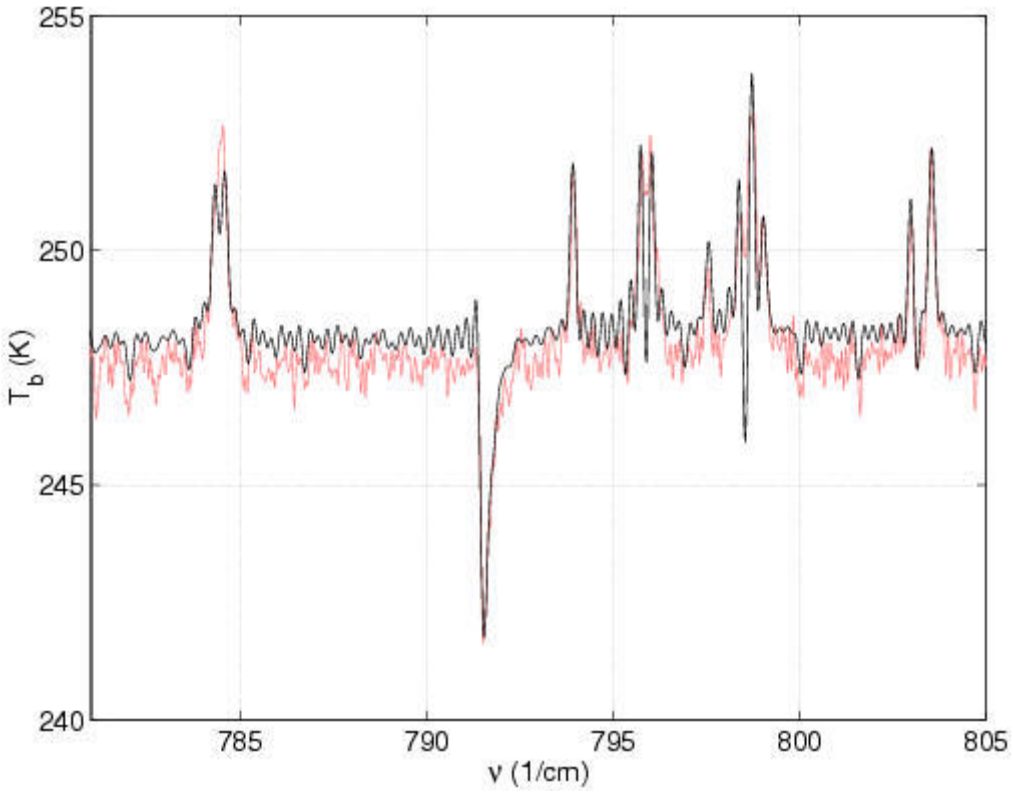

Figure 3. Low altitude temperature and water vapor inversions and skin/atmosphere temperature differences evident in weak water lines measured by IMG north of Pt. Barrow, Alaska, on December 11, 1996, (solid gray curve) and a line-by-line calculation (solid black curve) performed using a National Weather Station (NWS) radiosonde and Toth water vapor line parameters as input.

Atmospheric State

The accuracy of the atmospheric state data used as input to the line-by-line calculations is extremely important to the outcome of this analysis. In particular, errors in the input water vapor profile translate almost directly into errors in the derived spectral line strengths and widths, and into the interpretation of the accuracy of the published parameters. During the 1997 WVIOP, a large number of integrated and profiling water vapor measurements were made. For this analysis, the water vapor profiles were constructed using a combination of observations including radiosondes, in situ observations with chilled mirrors on the ground and on a tower at 25 meters and 60 meters, Raman Lidar, and column integrated water vapor derived from a Microwave Radiometer. Temperature profiles are taken from operational retrievals performed using a combination of AERI and Geostationary Observational Environmental Satellite (GOES) observations (Feltz et al. 1998).

Data Analysis and Preliminary Results

Several case studies have been constructed using the radiance and atmospheric state information. Homogeneous, clear-sky, nighttime periods are identified to produce low-noise, averaged spectra.

Line-by-line calculations are then performed using the input profiles, reduced to the appropriate spectral resolution, and compared to the radiance observations. In the calculations, absorption due to all gases other than water vapor is computed with Line-By-Line Radiative Transfer Models (LBLRTMs) (Clough et al. 1992). Water vapor absorption is computed using the CKDv2.3 water vapor continuum model and the corresponding local Lorentz/Voigt lineshape. A sample result obtained using a case study from September 16, 1997, is shown in Figure 4. This figure shows the effect of using the high resolution transmission (HITRAN'98) (Rothman et al. 1998) line parameters versus recent measurements of the line parameters by R. A. Toth, Jet Propulsion Laboratory (personal communication, 1994), as compared to AERI and AERI-X for the 775 cm^{-1} to 810 cm^{-1} region. A detailed examination of these comparisons for the entire spectrum yields information regarding the accuracy of individual lines.

Further analysis includes the determination of individual spectral line intensities and air-broadened Lorentz widths from the observations. This requires iteration of the calculation in a non-linear least squares algorithm whereby the line parameters are adjusted to minimize the difference between the measured and calculated radiances. An additional parameter that decouples the determination of the line parameters from errors in the continuum absorption and from small errors in the input profile is varied. This is done on a line-by-line basis and is most robust for spectral regions that are dominated by a single absorption line. A sample fit is shown in Figure 5 for a line at 784.46 cm^{-1}. For this particular line, the fitted parameters are in good agreement with the Toth values.

Conclusions and Future Work

The ability to measure spectral line intensities and air-broadened Lorentz widths from high spectral resolution, ground-based measurements has been demonstrated. Further analyses will yield a set of spectral regions and line parameters, which can be used for incorporation in to several remote sensing applications. The determination of the line parameters from the radiance measurements is, however, subject to the accuracy of the input temperature and water vapor profiles used in the analysis. On the other hand, once the line parameters are determined and verified from a set of carefully selected case studies, the radiance measurements can be used to assess the accuracy of the atmospheric state with high accuracy using the same spectral regions. Specific applications include the on-line/off-line surface temperature/emissivity retrieval from space, improvements in water vapor retrievals from AERI radiances, and boundary layer retrievals from satellite. With respect to the AERI retrieval work, selected weak water vapor spectral line regions will be incorporated into the retrieval algorithm with the goal of extending the retrievals to higher altitudes and improving the accuracy of the retrieved integrated column water vapor.

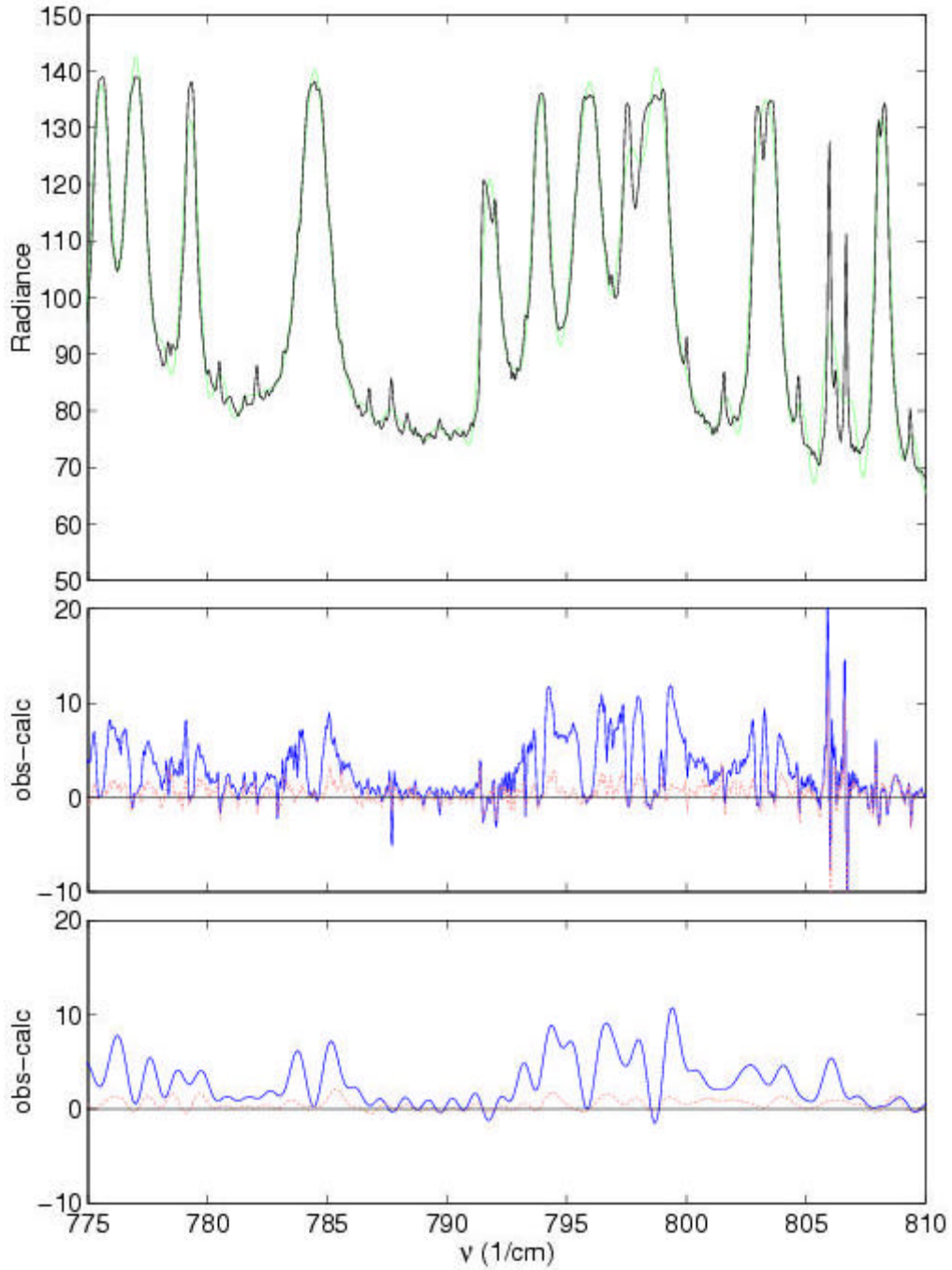

Figure 4. Downwelling radiances (top panel) measured by AERI-X (black curve) and AERI (gray curve) at the ARM SGP site on September 16, 1997, from 4 Universal Time Coordinates (UTC) to 5 UTC and differences between observed and calculated radiances using HITRAN'98 (black curves) and Toth (gray curves) water vapor spectral line parameters at AERI-X (middle panel) and AERI (bottom panel) resolution.

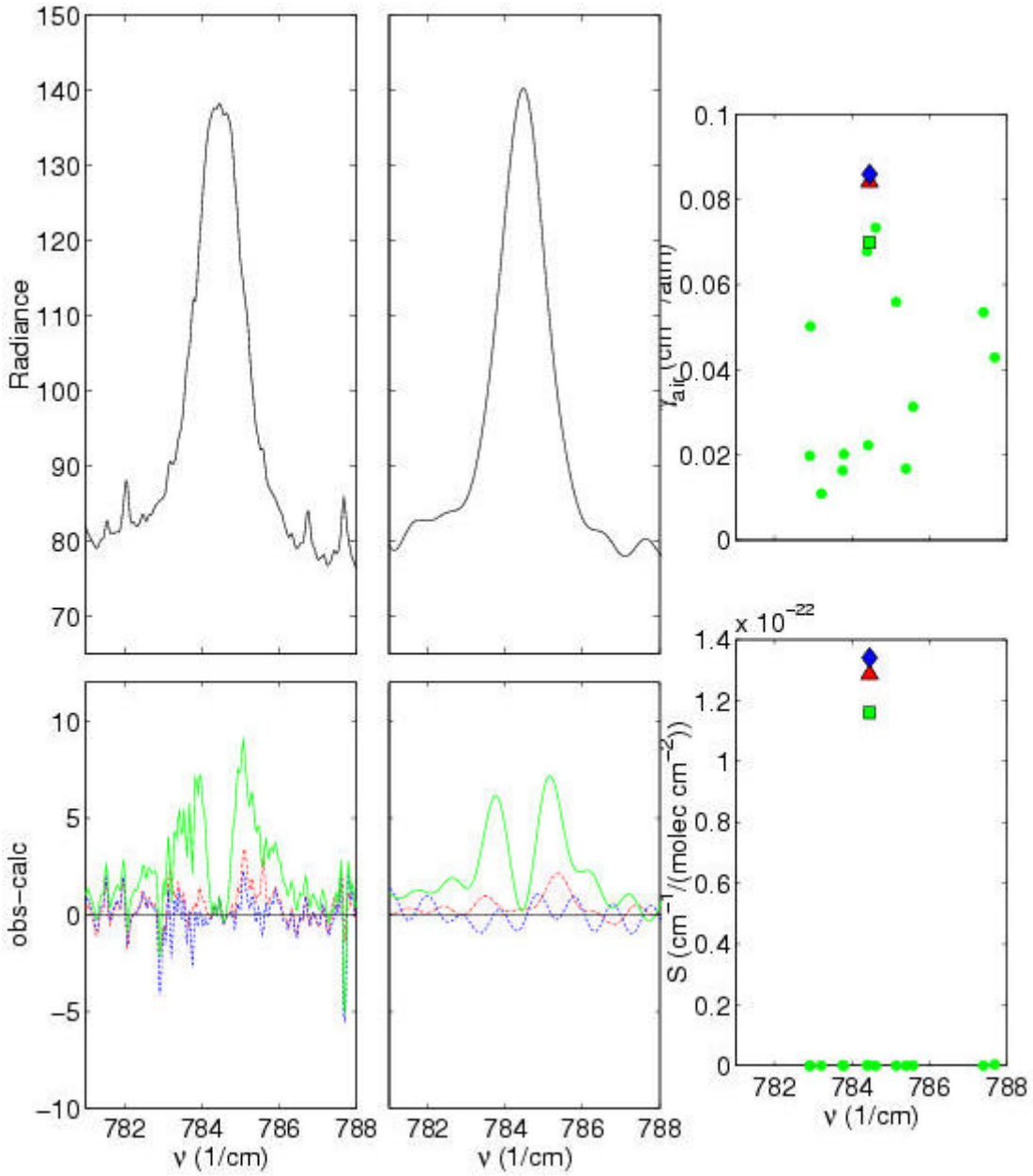

Figure 5. Determination of the intensity and air-broadened Lorentz width of a pure rotational transition of water vapor at 784.46 cm^{-1} using AERI-X and AERI measurements from September 16, 1997. The left-most plots show the AERI-X measurement and observed minus calculated radiances using HITRAN'98 (solid curve), Toth (dash-dot curve), and the fitted (dashed curve) line parameters; the middle plots are the analogous AERI measurement and differences; the right-most plots show the line intensities and air-broadened line widths (HITRAN, square; Toth, triangle; fitted, diamond).

References

Clough, S. A., M. J. Iacono, and J. L. Moncet, 1992: Line-by-line calculations of atmospheric fluxes and cooling rates: Application to water vapor. *J. Geophys. Res.*, **97**, 15,761-15,785.

Feltz, W. F., W. L. Smith, R. O. Knuteson, H. E. Revercomb, H. B. Howell, and H. M. Woolf, 1998: Meteorological applications of temperature and water vapor retrievals from the groundbased Atmospheric Emitted Radiance Interferometer (AERI). *J. Appl. Meteor.*, **37**, 857-875.

Ferrare, R. A., S. H. Melfi, and D. O'.C. Starr, 1995: A comparison of water vapor measurements made by Raman Lidar and radiosondes. *J. Atm. Ocean. Tech.*, **12**, 1177-1195.

Liljegren, J. C., E. R. Westwater, and Y. Han, 1997: A comparison of integrated water vapor sensors: WVIOP-96. In *Proceedings of the Seventh Atmospheric Radiation Measurement (ARM) Science Team Meeting*, CONF-970365. U.S. Department of Energy, Washington, D.C.

Moritz, R. E., J. A. Curry, A. S. Thorndike, and U. Untersteiner (Eds), 1993: Prospectus –SHEBA, a research program on the Surface Heat Budget of the Arctic Ocean, ARCSS-OAII Report \#3, 34 pp., ARCSS-OAII Sci Mgt. Ofc., Univ. Washington.

Murcray, F., T. Stephan, and J. Kosters, 1996: Instrument development for ARM: Status of the Atmospheric Emitted Radiance Interferometer-Extended Resolution (AERI-X), the Solar Radiance Transmission Interferometer (SORTI), and the Absolute Solar Transmission Interferometer (ASTI). In *Proceedings of the Fifth Atmospheric Radiation Measurement (ARM) Science Team Meeting*, CONF-9503140. U.S. Department of Energy, Washington, D.C.

Revercomb, H. E., W. F. Feltz, R. O. Knuteson, D. C. Tobin, P. F. W. van Delst, and B. A. Whitney, 1998: Accomplishments of the water vapor IOPs: An overview. In *Proceedings of the Eighth Atmospheric Radiation Measurement (ARM) Science Team Meeting*, DOE/ER-0738. U.S. Department of Energy, Washington, D.C.

Revercomb, H. E., W. L. Smith, R. O. Knuteson, F. A. Best, R. G. Dedecker, T. P. Dirkx, R. A. Herbsleb, G. M. Buchholtz, J. F. Short, and H. B. Howell, 1994: AERI – Atmospheric Emitted Radiance Interferometer. Paper presented at the *Eighth Conference on Atmospheric Radiation*, Am. Meteorol. Soc., Nashville, Tennessee, January 23-28, 1994.

Rothman, L. S. et al., 1998: The 1998 HITRAN molecular spectroscopic database and HAWKS (HITRAN Atmospheric Workstation). *J. Quant. Spectrosc. Radiat. Transfer*. In press.

Salisbury, J. W., D. M. D'Aria, and A. E. Wald, 1994: Measurements of thermal infrared spectral reflectance of frost, snow, and ice. *J. Geophys Res.*, **99**, 24,241-24,250.

Shimota, A., H. Kobayashi, and S. Kadokura, 1999: Radiometric calibration for the airborne interferometric monitor for greenhouse gases simulator. *Appl. Opt*., **38**, 571-576.

Smith, W. L., H. E. Revercomb, H. B. Howell, H. L. Huang, R. O. Knuteson, E. W. Koenig, D. D. LaPorte, S. Silverman, L. A. Sromovsky, and H. M. Woolf, 1990: GHIS –the GOES high-resolution interferometer sounder. *J. Appl. Meteorol*., **29**, 1189-1201.

Stokes, G. E., and S. E. Schwartz, 1994: The Atmospheric Radiation Measurements (ARM) Program: Programmatic background and design of the cloud and radiation testbed. *Bull. Am. Meteorol. Soc.*, **75**, 1201-1221.